ACS APPLIED MATERIALS & INTERFACES

Research Article

www.acsami.org

Injection Molded Polymeric Micropatterns for Bone Regeneration Study

Erika Zanchetta,[†] Enrica Guidi,[‡] Gioia Della Giustina,[†] Marco Sorgato,[†] Mauro Krampera,[§] Giulio Bassi,[§] Rosa Di Liddo,[‡] Giovanni Lucchetta,[†] Maria Teresa Conconi,[‡] and Giovanna Brusatin*[,†]

[†]Department of Industrial Engineering, University of Padua, Padua 35131, Italy

[‡]Department of Pharmaceutical and Pharmacological Sciences, University of Padua, Padua 35131, Italy

[§]Section of Hematology, Department of Medicine, University of Verona, Verona 37129, Italy

Supporting Information

ABSTRACT: An industrially feasible process for the fast mass-production of molded polymeric micro-patterned substrates is here presented. Micro-structured polystyrene (PS) surfaces were obtained through micro injection molding (μIM) technique on directly patterned stamps realized with a new zirconia-based hybrid spin-on system able to withstand 300 cycles at 90 °C. The use of directly patterned stamps entails a great advantage on the overall manufacturing process as it allows a fast, flexible, and simple one-step process with respect to the use of milling, laser machining, electroforming techniques, or conventional lithographic processes for stamp fabrication. Among the different obtainable geometries, we focused our attention on PS replicas reporting 2, 3, and 4 μm diameter pillars with 8, 9, 10 μm center-to-center distance, respectively. This enabled us to study the effect of the substrate topography on human mesenchymal stem cells behavior without any osteogenic growth factors. Our data show that microtopography affected cell behavior. In particular, calcium deposition and osteocalcin expression enhanced as diameter and interpillar distance size increases, and the 4-10 surface was the most effective to induce osteogenic differentiation.

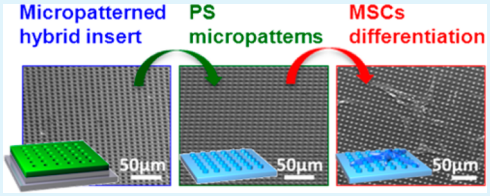

KEYWORDS: *polystyrene micropatterns, microinjection molding, stem cells, hybrid sol−gel system, osteogenesis of hMSCs*

1. INTRODUCTION

The physical and chemical properties of materials in the local cellular microenvironment are increasingly appreciated as key players in stem-cell fate decisions, that is the cell ability of self-renewing and differentiating.[1] Cells interact with surfaces typically through the creation of attachment points linking the cytoskeleton (cell's mechanical framework) to extracellular binding sites. For this reason the basic understanding of cell−substrate interaction represents a crucial factor in the fields of tissue engineering, drug development, and regenerative medicine (tissue engineering and cell therapy).[2,3] Traditionally, substrate materials were simply considered as inert context that carry biochemical supplements (such as growth factors) for cell growth, differentiation promotion, or both. However, more recently, intrinsic material properties that mimic physiologically relevant extracellular matrix (ECM) characteristics have been proven to regulate stem cell fate (from adhesion to proliferation and differentiation). In particular, substrate mechanical stiffness,[4,5] micro- and nanometer-scale topography,[6,7] and simple chemical functionality[8] each have been reported to play a fundamental role in driving human mesenchymal stem cell (hMSC) differentiation.[9] Topography was first identified to influence cell behavior as early as 1911, when the guidance of cells along the fibers of a spider's web was observed:[10] the cells followed the fibers of the web in a phenomenon called stereotropism, or physical guidance. Since this discovery, numerous studies have been conducted to analyze cell behavior on various micro- and nano-features such as lines, wells, holes, and more. After that, topography, independent from substrate chemistry, was found not only to have a strong effect on cell morphology,[11,12] but also to provide physical, geometrical, mechanical, and structural signals that act together as a smart entity for guiding cell adhesion,[13] orientation,[14] migration, proliferation,[15,16] viability,[17] cytoskeletal organization, gene expression, and differentiation.[18] Moreover, MSCs specify lineage and commit to phenotypes with extreme sensitivity to tissue level elasticity. Soft matrixes that mimic brain are neurogenic, stiffer matrixes that mimic muscle are myogenic, and comparatively rigid matrixes that mimic collagenous bone prove osteogenic.[4,5]

According to this, influencing cell behavior from proliferation to differentiation using the material design of the substrate or implant topography has been found to be a desirable approach for many regenerative medicine applications. As an example, the development of a new family of implantable bioinspired materials that better mimic the natural bone extracellular matrix, a naturally nanocomposite tissue, can stimulate stem cell differentiation toward osteogenic lineages in the absence of

Received: January 16, 2015
Accepted: March 10, 2015
Published: March 10, 2015

DOI: 10.1021/acsami.5b00481
ACS Appl. Mater. Interfaces 2015, 7, 7273−7281

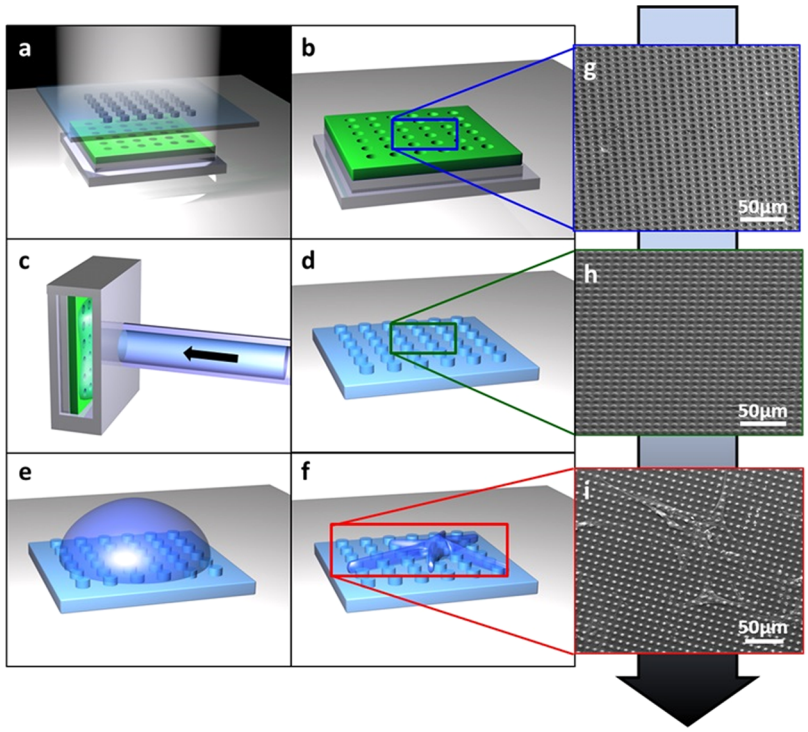

Figure 1. Direct realization of micro structured stamps for μIM through UV lithography: (a) spin coating of TMSPM-Zr solution on the metallic substrate and UV-exposure of the film through a mask reporting the required structures; (b) final stamp obtained after development; (c) micro injection molding of PS substrates using the zirconia-based directly patterned stamp; (d) PS microstructured stamp obtained with μIM; (e) MSC adhesion on the PS microstructured substrate; (f) MSC differentiation into osteoblasts on the PS microstructured substrate; (g) SEM image of the microstructured hybrid stamp; (h) the PS replica; and (i) cells adhered onto the PS substrate.

specific chemical treatments.[19] In particular, interactions between MSCs and surfaces with specific micro- and nanopatterns can stimulate the cells to produce in vitro bone mineral.[20,6]

Specific trends with regard to the influence of the topographical effect on cellular behavior are, however, challenging to establish,[21] and generally, several substrates are needed to identify the effect on cell proliferation and differentiation induced by distinct surface topographies, for example, through combinatorial screening approach.[22] To this end, the interest in developing manufacturing systems that make it possible to produce polymeric micro- and nano-substrates at a reasonable price and in large numbers, in order to create the operational basis for an industrial production, is continuously increasing.

In this contribution, micro injection molding (μIM) technique[23−25] has been chosen as an industrially viable processes for the accurate and cost-effective mass production of molded micro-patterns realized in polystyrene (PS) not treated for cell cultures, a well-established biocompatible material for on-chip cell culture.[26,27] A great advantage of our proposed approach is the realization of the μIM stamps through the direct photopatterning of a zirconia-based hybrid organic−inorganic spin-on system (hereafter referred to as TMSPM-Zr) on flat metallic surfaces (Figure 1a,b), moving the overall manufacturing process toward the final step of industrialization with respect to the use of mold tools obtained through traditional lithographic techniques.[28] Among different tested resists, we chose the zirconia-based material for its high mechanical, thermal, and fatigue resistance, as it withstands 300 cycles at 90 °C without failure. It must be pointed out that in a market characterized by low added value products, a durable, low-cost master mold with well-fabricated micro/nanoscale structures is a critical point for mass production with the micro injection molding process. The manufacture of the mold generally relies on expensive, time-consuming manufacturing technologies that can create the necessary micro structures, withstanding 10^3−10^6 cycles, but are generally characterized by low material removal rate (MRR), for example, milling, laser machining, and electroforming.[29−31] Therefore, the need for cheap micro- and nanostructured inserts obtained with engineered materials as alternative inserts to the metallic tools for micro injection molding process is increasing.

The use of directly patterned materials brings about some advantages with respect to conventionally used micromachined metallic stamps or traditional lithographic procedures: (1) an easier, versatile (changes of geometries can be realized in acceptable time, according to mask availability), time- and cost-effective fabrication process,[32,33] (2) stamps characterized by a low thermal dispersion that allows to maintain the temperature of the stamps during the μIM replication process, and (3) the possibility of realizing several structures with no grain size limitations to the final resolution and a better surface finishing, typical problems of metallic insert and of some micro machining tools.

Herein, stamps reporting different microfeatures (2, 3, and 4 μm diameter holes with 8, 9, and 10 μm center-to-center distance, respectively) were fabricated in order to obtain several corresponding PS replicas in a short time through micro-injection molding (Figure 1c,d). Then, the effects of the substrate topography on hMSCs adhesion, proliferation, and osteogenic differentiation were investigated in the absence of inductive growth factors (Figure 1e,f).

DOI: 10.1021/acsami.5b00481
ACS Appl. Mater. Interfaces 2015, 7, 7273−7281

2. EXPERIMENTAL METHODS

2.1. Materials: TMSPM-Zr Synthesis. 3-(Trimethoxysilyl)propyl methacrylate (TMSPM) was hydrolyzed in acidic conditions (1% molar of HCl with respect to TMSPM) at room temperature. Zr-butoxide ($Zr(OBut)_4$) and metacrylic acid (MAA) were separately left stirring for 5 min. The two starting silica and zirconia precursor solutions were then mixed together and left stirring for 1 h. The molar ratios between the precursors were TMSPM:$Zr(OBut)_4$:MAA = 1:0.5:1. Tetrahydrofuran (THF) was finally added to achieve the desired concentration, and the solution was filtered through a microporous membrane (0.2 μm Millipore) to get a better film quality after spin coating.

Hybrid films were deposited on cleaned silicon wafer (100) by spin coating technique at different spin speeds according to the final wanted thickness. As reported in Figure S1 (Supporting Information), a wide interval of thicknesses, ranging from some microns to a few hundred nanometers, could be obtained by spin-coating the synthesized solution at different concentrations. This aspect would enable us to realize μIM stamps with different features size to fit the requirements of a great number of applications.

2.2. Hybrid System Lithography. The UV patterning of TMSPM-Zr was induced by exposing the spin-coated films through a mask possessing the final required structures, that is, 2, 3, and 4 μm diameter dots with 8, 9, and 10 μm center-to-center distance, respectively. The UV lamp used for patterning was the 250 nm enhanced type Xe−Hg Hamamatsu Lightningcure LC5 whose emission spectrum (red line) is overlapped to TMSPM-Zr absorption spectrum in Figure 2. The TMSPM-Zr solution absorbs the higher

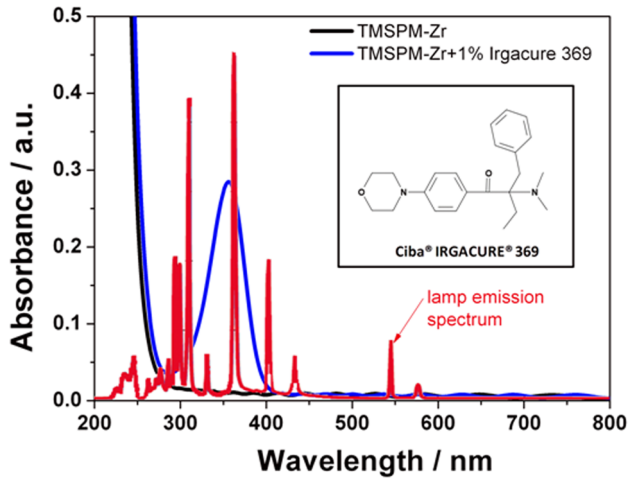

Figure 2. UV−vis absorption spectra of TMSPM-Zr (black line) without and (blue line) with 1% molar with respect to TMSPM of IRGACURE 369. (red line) The Hamamatsu Lightningcure LC5 lamp spectrum is also reported for comparison. (Inset) Chemical structure of IRGACURE 369.

energy radiation emitted by the lamp (below 270 nm). The radical photopolymerization of the acrylic groups under UV exposure was controlled by the addition of a commercial photoinitiator, 2-benzyl-2-dimethylamino-1-(4-morpholinophenyl)-butanone-1 (Ciba IRGACURE 369), with a molar concentration of 1% with respect to TMSPM. Figure 3 reports the UV−Visible absorption spectra of TMSPM-Zr films without (black line) and with 1% molar (with respect to TMSPM) of photoinitiator (blue line) obtained with a UV−vis spectrometer (JASCO V-570) in the wavelength range 200−800 nm: the addition of the photoinitiator clearly allows to absorb the lower emission energies of the lamp used for patterning. The photoinitiator chemical structure is shown in the inset.

The chemical modifications occurring in the film upon UV irradiation were evaluated from the Fourier transform infrared spectra (spectrometer Jasco FT-IR-620) in the range of 400−4500 cm^{-1} with a resolution of ±4 cm^{-1}. The first set of lithographic tests and the dose matrix experiments were conducted using silicon substrates spin-coated at different speeds with the solution diluted in THF to easily adjust film thicknesses in the 1−6 μm range. After selecting the optimal lithographic process parameters, we fabricated the final hybrid microstructured stamps on circular or rectangular pieces of steel 39NiCrMo3 for injection molding. The optimal exposure conditions were selected depending on the hybrid film thickness between 3 and 11 J/cm^2 UV dose (measured between 260 and 400 nm range wavelength). The films were then developed for 15 s in a mixture of ethanol and acetone (100:1 v/v). Finally, after development, the films were dried by blowing air and hard-baked at 100 °C for 1 h, with heating rate of 1 °C/min, and the obtained results were inspected by scanning electron microscope SEM (FEI QUANTA 450).

2.3. Experimental Setup of Microinjection Molding. For the molding experiments, a state-of-the-art μIM machine (MicroPower 15 from Wittmann Battenfeld) was used. The machine is characterized by a maximum clamping force of 150 kN and a maximum injection speed of 750 mm/s. Unlike conventional injection molding machines, the MicroPower 15 has an injection system composed of a screw with a diameter of 14 mm and a separate plunger injection unit with a diameter of 5 mm.

The mold cavity considered in this study is placed at the end of a trapezoidal cold runner 16 mm long, 3−2 mm wide, and 1.5 thick, connected through a rectangular gate 0.3 mm long, 2.7 mm wide, and 0.5 mm thick.

The material used for injection molding was a commercial polystyrene resin PS Crystal 1540, manufactured by TOTAL, with a melt flow index (MFI; 200 °C, 5 kg) of 12 g/10 min and a T_g of 100 °C. PS has been selected due to its known good biocompatibility, high flowability, and high transparency. Furthermore, polystyrene was not treated for cell cultures to better discriminate the effects of micropillared on cell adhesion and growth.

To investigate the influence of the controllable process variables on the replication capability (screening phase), a three-level full factorial plan was performed. According to literature[34] the following three factors were selected: mold temperature (T_{mold}), injection speed (V_{inj}), and holding pressure (P_{pack}). The range values for each factor (Table 1) were defined considering the literature, recommendations of the material supplier and technological limits of the available experimental setup; the melt temperature and the holding time were fixed at 240 °C and 20 s, respectively. During injection molding experiments, an automatic execution of the process (including part ejection and handling) was performed for each treatment. First, 50 cycles were carried out to stabilize the process. Subsequently, 10 parts obtained from the following 30 cycles have been randomly collected and analyzed to establish the best molding parameters.

The response variable for this analysis was chosen to be the replicated height of the pillars, measured by means of a state-of-the-art 3D optical profiler (Sensofar PLu neox) operating in confocal mode with 20× and 100× objectives.

2.4. Cell Cultures. MSCs were obtained from bone marrow (BM) aspirates of healthy donors, after written informed consent, as approved by the Ethics Committee of Azienda Ospedaliera Universitaria Integrata Verona (N. Prog. 1828, May 12, 2010; 'Institution of cell and tissue collection for biomedical research in Onco-Hematology'). BM mononuclear cells were separated by density gradient centrifugation and cultured with proliferation medium containing α-minimal essential medium (α-MEM, Life Technologies, Baltimore, MD), 18% fetal bovine serum 16000 (FBS 16000, Life Technologies), 1% glutamine (Sigma, St. Louis, MO), and 1% penicilline/streptomycine (Sigma). Cells were grown at 37 °C in a humid atmosphere with 5% CO_2. The medium was refreshed three times a week. Immunophenotype and differentiation potential were assessed as previously reported.[35] MSCs were used until the fourth passage and harvested at 80% confluence. Cells (1.5×10^4 cells/cm^2) were seeded on pillar-structured polystyrene arrays previously put onto wells of 96-well plates and cultured with α-MEM supplemented with 10% FBS 16000, 1% glutamine, and 1% penicilline/streptomycine. Cultures grown on flat injection molded polystyrene

DOI: 10.1021/acsami.5b00481
ACS Appl. Mater. Interfaces 2015, 7, 7273−7281

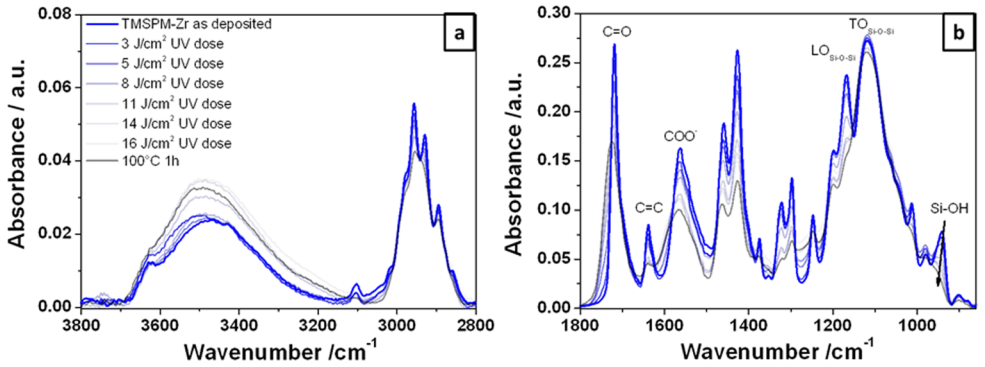

Figure 3. FTIR spectra of TMSPM-Zr films exposed to increasing UV dose and following thermal treatment at 100 °C for 1 h in the (a) 3800−2800 and (b) 1800−860 cm^{-1} wavenumber range.

Table 1. Process Parameters Settings of the Screening Plan

factor	low level	medium level	high level
T_{mold} (°C)	50	70	90
P_{pack} (bar)	100	150	200
V_{inj} (mm/s)	200	350	500

substrates were used as control. After various time points from seeding, cell morphology, adhesion, proliferation, and osteogenic differentiation were evaluated.

2.4.1. Scanning Electron Microscopy (SEM). At various time points from seeding, cultures were fixed in 3.7% formaldehyde for 20 min at room temperature and then dehydrated with a graded ethanol series. After gold sputtering, samples were observed using a scanning electron microscope (JEOL JSM-6490).

2.4.2. MTS Assay. To test cell viability, we used the 3-(4,5-dimethylthiazol-2-yl)-5-(3-carboxymethoxyphenyl)-2-(4-sulfophenyl)-2*H*-tetrazolium) (MTS) test (CellTiter 96 AQueous One Solution Cell Proliferation Assay; Promega, Austria), according to the manufacturer's instructions. Briefly, at 24 h and 3, 7, 14, and 21 days from seeding, 200 μL of cell media, containing 10% MTS, were added into each well, and cells were incubated at 37 °C for 4 h. Optical density of purple formazan produced in living cells was measured at 490 nm, using a Microplate autoreader EL 311 (BIO-TEK Instruments, Inc., Winooski, VT). Results were expressed as number of cells. The linearity of absorbance of formazan over a range of 2.5×10^3 to 20×10^3 cells was established by determining the linear coefficient (0.999).

2.4.3. Alizarin Staining. At 7, 14, and 21 days from seeding, cultures were rinsed with phosphate buffered solution and fixed in 3.7% formaldehyde. To each well was then added 40 mM Alizarin red solution (Alizarin Red S, Sigma-Aldrich), which was then incubated at room temperature for 20 min.[36] The dye was extracted by 10% acetic acid (200 ul/well). Acetic solutions were heated at 85 °C and lyophilized using Savant (Savant Speed Vac Concentrator, Thermo Scientific, Rockford, IL). Each sample was then resuspended in 10% acetic acid (pH 4.1), and optical density was determined at 405 nm using a Microplate Autoreader EL 311. Results were expressed as μM alizarin.

2.4.4. Reverse Transcription Polymerase Chain Reaction (RT-PCR). At 21 days, total RNA was extracted using TRIzol method according to the manufacturer's instructions (Invitrogen, Paisley, United Kingdom) and quantified using NANODROP 2000 (Thermo Scientific). Primers were obtained from Invitrogen, and their sequences are reported in Table 2. Glyceraldehyde 3-phosphate dehydrogenase (GAPDH) was chosen as the housekeeping gene. RT-PCR was carried out through the Qiagen One Step RT-PCR Kit (Qiagen, Crawley, United Kingdom) according to manufacturer's protocol and using total RNA at concentration of 500 ng/reaction for each sample. The thermal cycling program consisted of 50 °C for 30 min (reverse transcription), 95 °C for 15 min (DNA-polymerase activation), 40 two-step cycles of 95 °C for 30 s (denaturation), 50 °C for 1 min (annealing) and 72 °C for 1 min (elongation). The procedure was carried out using the iCycler iQ (Bio Rad). Table 2 shows the primer sequences used for PCR amplification. To obtain a semiquantitative assessment of gene expression, data were expressed as normalized ratios by comparing the integrated density values for osteocalcin (OC) gene with those for GAPDH. The PCR products were separated by 2% agarose gel electrophoresis and visualized by Gel Red Nucleic Acid staining 1:10000 (Biotium, Hayward, California). Images of the gel were captured with Gel Doc Imager (Bio-Rad, Hercules, CA) and analyzed with Image Lab software (Bio-Rad).

2.4.5. Statistical Analysis. Triplicate experiments were performed. The results were expressed as the arithmetic mean ± standard deviation. Their statistical comparison was performed by analysis of variance, followed by Student's *t* test.

3. RESULTS AND DISCUSSION

3.1. UV Curing of the Hybrid Acrylate System. The photopolymerization process of TMSPM with the addition of Irgacure 369 is reported in Scheme S1 (Supporting Information). α-Amino-alkylphenones undergo a rapid photocleavage reaction that generates the highly reactive free radicals needed for the polymerization process initiation.[37]

The chemical changes that occur when TMSPM-Zr films are exposed to UV light and after the final thermal treatment at 100 °C were investigated by FTIR spectroscopy, as reported in Figure 3a,b. With an increasing UV irradiation dose and thermal treatment, the intensity of the band due to C═C bond at around 1640 cm^{-1} decreases, indicating that polymerization of TMSPM and MAA occurs. The trend of the peak at 1640 cm^{-1} at increasing UV doses in Figure S2 (Supporting Information) confirms that C═C photopolymerization is

Table 2. Primers for PCR Amplification

gene	abbreviation	primer sequence	accession
osteocalcin	OC	F: TCACACTCCTCGCCCTATT R: CCTCCTGCTTGGACACAAA	NM_199173.4
glyceraldehyde 3-phosphate dehydrogenase	GAPDH	F: ACCACAGTCCATGCCATCAC R: TCCACCACCCTGTTGCTGTA	NM_002046.5

DOI: 10.1021/acsami.5b00481
ACS Appl. Mater. Interfaces 2015, 7, 7273−7281

more effective with the addition of Irgacure 369 with respect to TMSPM-Zr film without photoinitiator when exposed to the same UV dose. All the other peaks related to the vinyl C−H stretch (3100, 3040, and 3020 cm^{-1}), in-plane bend (1425, 1324, and 1300 cm^{-1}), and out-of-plane bend (983 and 880 cm^{-1}) decrease as well. The peaks at 1547 cm^{-1}, ascribed to the COO^- band in a carboxylic acid salt formed through the reaction between Zr precursor and MAA,[38] shifts to higher wavenumbers in the UV-irradiated areas, and the intensity of the band becomes smaller: polymerization must induce different coordination states of COO^-. The peak related to the C═O bond typical of esters, such as TMSPM, at 1725 cm^{-1} shifts to higher wavenumbers and becomes broader due to the change of molecule configuration after C═C polymerization. The longitudinal (LO) and transverse (TO) optical components of the asymmetric Si−O−Si stretching vibrations ν_{AS}(Si−O−Si) can be identified at 1120−1170 and 1040−1070 cm^{-1}, respectively. Because the longitudinal optical component band of ν_{AS}(Si−O−Si) in normal incidence transmission spectroscopy is activated only thanks to the pore light scattering of the infrared radiation, such that a fraction of the absorbed light is effectively obliquely incident, the LO/TO ratio can be correlated with the free-volume or porosity of the coatings. Therefore, while the TO absorption of TMSPM-Zr film remains almost constant, the decrease of LO mode peaks indicates the densification of the coating with the subsequent lowering of porosity for increasing UV exposure and thermal treatment.[39] Finally, Si−OH sol−gel condensation is promoted by UV curing and thermal treatment as the absorption peak around 950 cm^{-1} decreases.

Therefore, the overall outcome of the UV exposure of the TMSPM-Zr hybrid resist is the organic component polymerization and the condensation of the inorganic network.

3.2. UV Lithography of the Hybrid Acrylate System. TMSPM-Zr hybrid resist showed a negative behavior, as the unexposed areas of the film dissolved in the selected development, that is, a mixture of 100:1 volume ratio of ethanol to acetone. The contrast curves of TMSPM-Zr 110 g/L solution deposited by spin coating at 2000 rpm for 30s (2 μm thick film) is reported in Figure 4: the residual thickness of the

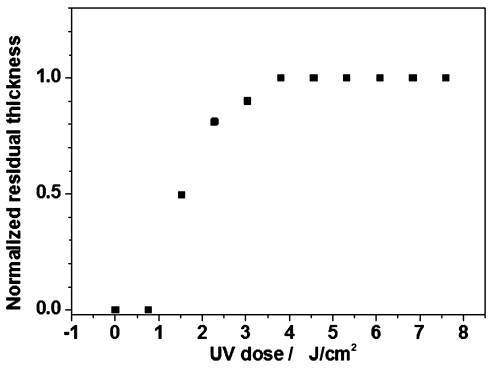

Figure 4. Contrast curve of 2 μm thick TMSPM-Zr film.

hybrid film after development (normalized to the initial thickness) is presented as a function of the applied UV exposure dose. In the investigated energy range, a dose of 4 J/cm^2 is required for preserving the 2 μm thick film after 15 s development, thus giving an approximate evaluation of the correct dose for UV lithography.

TMSPM-Zr 110 g/L solution was spin coated at 2000 rpm for 30 s on steel inserts of 1−2 cm^2 area to be housed in a custom-built steel mold for microinjection molding, as reported in Figure 5a. The hybrid films were exposed to a 4 J/cm^2 UV

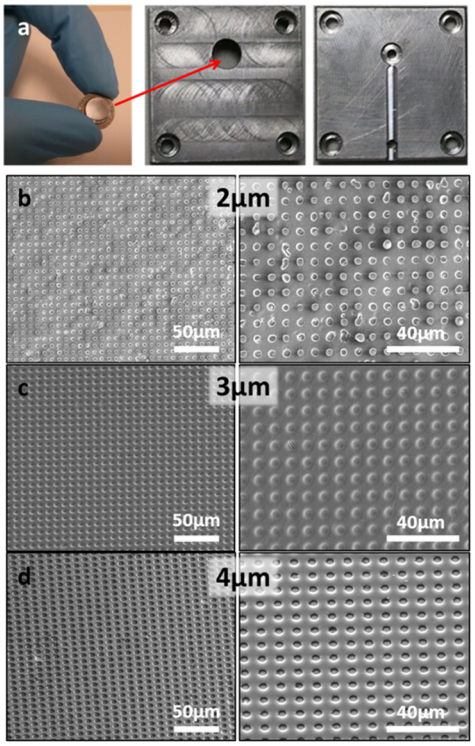

Figure 5. (a) Microstructured stamp to be housed in a custom-built steel mold for microinjection molding. SEM images at increasing magnification of inserts with (b) 2, (c) 3, and (d) 4 μm diameter structures patterned with UV lithography on TMSPM-Zr films.

dose through a quartz mask, revealing the wanted structures after development, and postbaked before being used as injection-molding stamps. Holes with 2, 3, and 4 μm diameters and 8, 9, and 10 μm center-to-center distances, respectively, were fabricated, as shown by SEM images in Figure 5b−d.

3.3. Microinserts Replication through Micro Injection Molding. We performed the three-level full factorial plan to identify the factors that mainly affect the replicated micro pillar height. The analysis of variance results indicated that all the factors and their interactions (in particular, the mold temperature) are significant, as reported in the literature.[16,40] The maximum replication degree is achievable for the high values of the factors, namely T_{mold} = 90 °C, V_{inj} = 500 mm/s, and P_{pack} = 200 bar.

An image of the PS substrate replicated with injection molding technique is reported in Figure 6a. The replication area was a circle of 6 mm diameter, chosen as the PS replicated substrates perfectly fit in the wells (6.4 mm) of a 96-well plate, used for cell culture. Figure 6b−d shows SEM images at two different magnifications of the PS microstructured surfaces reporting 2, 3, and 4 μm diameter pillars with 8, 9, and 10 μm center-to-center distance, respectively, and the corresponding 3D optical profiler images. The replication fidelity of the stamp can be appreciated from Figure S3 in the Supporting Information. Hereafter, we will refer to the different substrates with the following names (reported in Figure 6): 2-8 (2 μm diameter pillar and 8 μm center-to-center distance); 3-9 (3 μm

DOI: 10.1021/acsami.5b00481
ACS Appl. Mater. Interfaces 2015, 7, 7273−7281

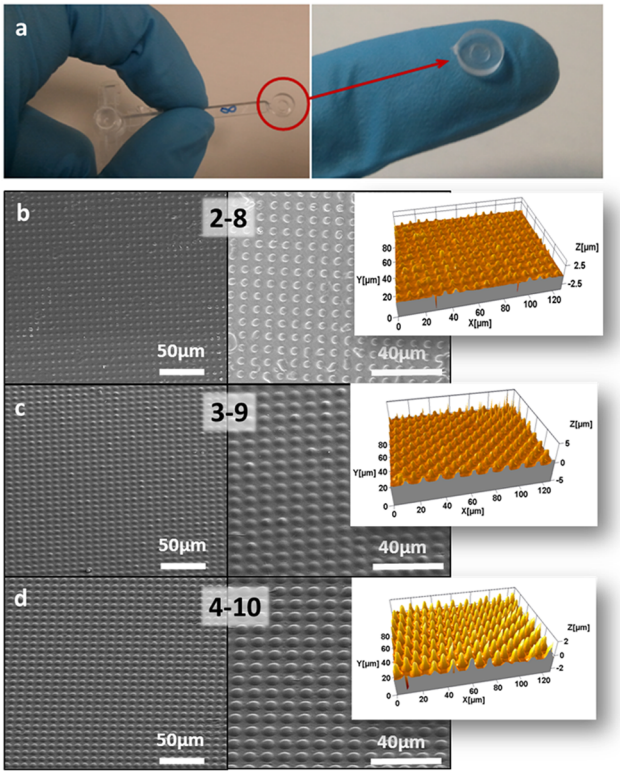

Figure 6. (a) Example of a PS microstructured substrate after injection-molding; (b–d) SEM images at increasing magnification (and corresponding 3D optical profiler images) of the PS replicated microstructured substrates reporting 2 (named 2-8), 3 (named 3-9), and 4 μm (named 4-10) diameter pillars.

diameter pillar and 9 μm center-to-center distance); 4-10 (4 μm diameter pillar and 10 μm center-to-center distance).

The great advantage of the hybrid stamp used is that it withstands 300 cycles at 90 °C, showing the best performance compared to other tested resists (as an example, Figure S4 of the Supporting Information shows the comparison with a micropatterned stamp obtained with SU8-2100 negative photoresist; MicroChem, Newton, MA). The durability of the zirconia-based insert during the micro injection molding process was experimentally investigated using the same process parameters utilized for the realization of the polymeric support for cell differentiation. The maximum target was fixed at 300 cycles. This value derives from the need to provide 200 samples for the cell cultures with a margin of 100 samples. An automatic execution of the process was performed, and we collected a molded sample every 10 cycles to analyze the failure of the mold insert. The results showed that there was not failure of the zirconia insert after 300 cycles, and neither the stamp microstructures were affected in terms of roughness.

3.4. Cell Adhesion. It is well-known that MSCs adhesion on biomaterials occurring through integrin receptors regulates growth and differentiation.[41] Surface topography modulating focal adhesion assembly and cytoskeletal stress can both activate signaling cascades and modify the organization of nuclear components, leading to changes in gene expression.[42] Cell adhesion was evaluated by means of SEM and MTS assay after 24 h from seeding on micropatterned and control substrates. It must be pointed out that control substrates were obtained by replicating a flat steel stamp with polystyrene with the same microinjection conditions selected for the microstructured surfaces. As shown in Figure 7, MSCs well adhered onto all types of arrays, showing an elongated shape. A more flattened phenotype was visible on control, compared to that observed on 3-9, 2-8, and 4-10 where cells showed an elongated shape (Figure 7A–D). It has been observed that a relationship exists between cell morphology and MSC differentiation, that is, high-spread cells are often committed to an osteoblastic fate.[43] The cell numbers on 2-8 and 3-9 were significantly lower than that determined in the control cultures grown on flat surfaces, whereas no variations were observed on 4-10. In all cultures, the number of cells was about 5-fold lower with respect to the seeding density (4.8×10^3 cells/array). The latter result was expected because all arrays were composed of polystyrene not treated for cell cultures.

SEM analysis revealed that on all surfaces cells formed an almost confluent monolayer at 7 days and then stratified at 14 and 21 days (Figure S5, Supporting Information, reports the SEM images for cell cultures on 2-8 surfaces, taken as example, after 72 h, 7 days, and 14 days of proliferation). In agreement with the morphological data, in all cultures, the cell number increased until 14 days of culture, whereas an overall slowdown of cell proliferation was evident between 14 and 21 days (Figure 8). Furthermore, at 21 days, the cell number on all pillar-structured polystyrene surfaces were significantly lower than that determined on control cultures. This data suggests that a shift in cell cycle toward a phase of cell differentiation may have occurred on microstructured surfaces.

3.5. Osteogenic Differentiation of hMSC. Osteogenic differentiation of hMSCs was verified by evaluation of calcium

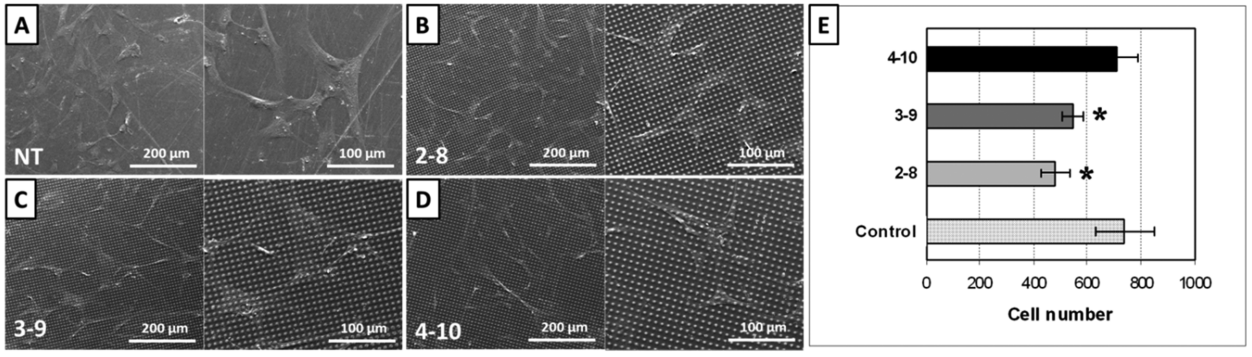

Figure 7. Cell adhesion on pillar-structured polystyrene surfaces and control ones at 24 h after seeding. SEM micrographs at two different magnifications: (A) control; (B) 2-8; (C) 3-9; and (D) 4-10. (E) MTS assay; results, expressed as cell number, are means ± SD of three independent experiments; * = $p < 0.05$ vs control cultures, Student's t test.

DOI: 10.1021/acsami.5b00481
ACS Appl. Mater. Interfaces 2015, 7, 7273–7281

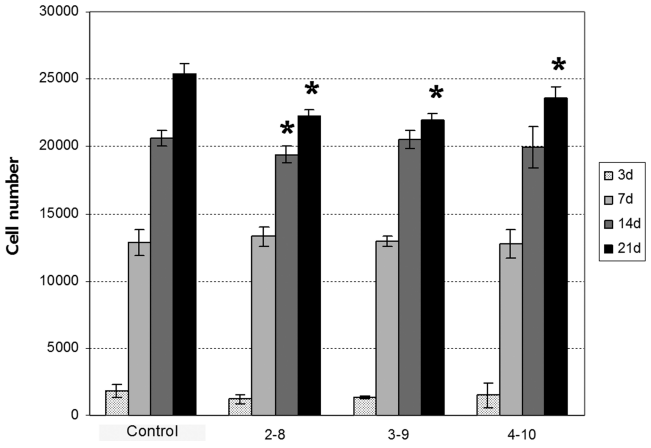

Figure 8. Cell proliferation at 3, 7, 14, and 21 days after seeding on pillar-structured polystyrene surfaces and control ones. Results, expressed as cell number, are means ± SD of three independent experiments. * = $p < 0.05$ vs control cultures, Student's t test.

deposition and osteocalcin mRNA expression. Figure 9 shows that cells possessed mineralization capacity since alizarin was detected also in cultures grown on control surfaces, and its concentration increased during the culture period, similarly to that occurred on pillar-structured surfaces. At 7 and 14 days after seeding, low levels of mineralization were measured on all surfaces, whereas stain concentration greatly enhanced at 21 days. Furthermore, at the latter time point, calcium deposition was significantly higher on 3-9 and 4-10 in comparison to that observed in control cultures.

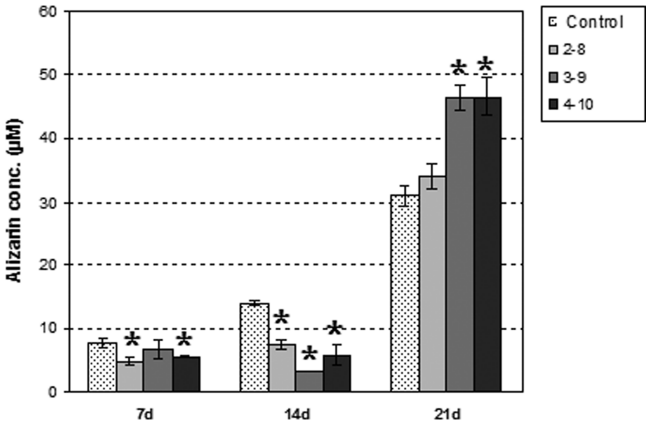

Figure 9. Effects of pillar-structured surfaces on mineralization of MSCs at 7, 14, and 21 days after seeding. Results, expressed as μM alizarin, are means ± SD of three independent experiments. * = $p <$ 0.05 vs control cultures, Student's t test.

At 21 days from seeding, MSCs grown on 2-8 and control surfaces showed low levels of 113 bp PCR product coding for OC mature form (Figure 10A). On the contrary, cells cultured on 3-9 and 4-10 also presented a 540 bp PCR product that codes for OC precursor. Densitometric analysis revealed that the expression of both OC mRNAs was significantly higher in cells grown on 3-9 and 4-10 than those determined in control cultures. Furthermore, the highest expression levels were detected in 4-10 cultures. Taken together, calcium deposition and osteocalcin mRNA expression indicate a relationship between osteogenic differentiation and diameter and interpillar distances.

4. CONCLUSIONS

Mass-production of micropillared polystyrene surfaces was realized through the micro injection molding process for hMSCs proliferation and differentiation into bone minerals, because a mandatory requirement for cell culture screening is the high substrate number needed. Directly patternable silica–zirconia hybrid materials enabled us to easily obtain micro-structured mold inserts for micro injection molding with different geometries and the ability to withstand 300 cycles at 90 °C.

Collectively, our data demonstrated that the microstructure influences the behavior of MSCs. An elongated cell shape was observed on cultures grown on the modified surface, showing osteogenic potential in the absence of growth factors commonly used to induce osteoblast differentiation. Although no clear relationships among cell adhesion and proliferation and microstructural size were detected, our results clearly indicate that the mineralization and OC expression enhanced as diameter and interpillar distance size increases. Our results agree with those of Kolind et al.,[44] who observed that the increase in the interpillar gap enhances the expression of osteogenic markers in human mesenchymal dental-pulp-derived

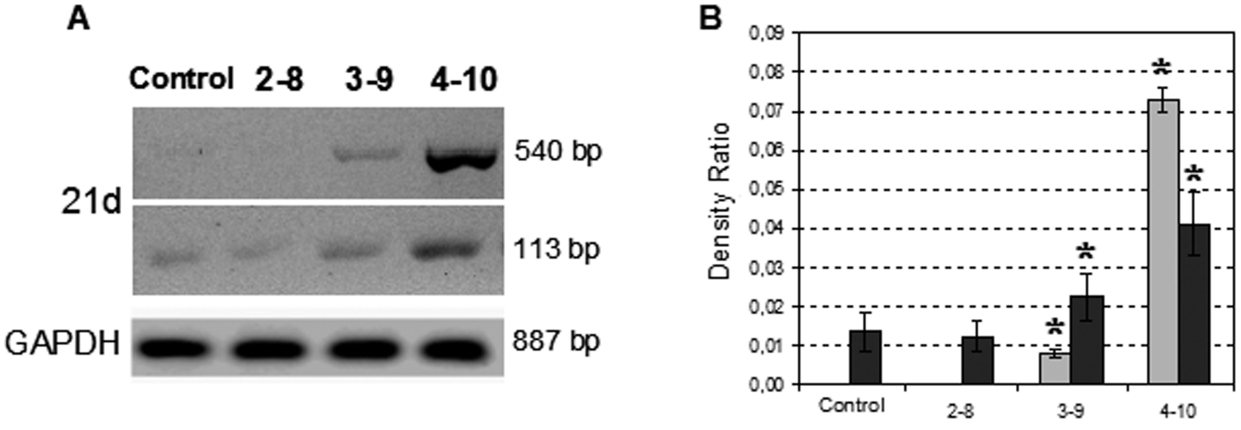

Figure 10. Effects of pillar-structured surfaces on OC mRNA expression of MSCs at 21 d after seeding. (A) Representative agarose gel of the PCR products. (B) Densitometric analysis of the PCR products, normalized with the corresponding GAPDH value; (black) 113 bp and (gray) 540 bp. Results, expressed as density ratio, are means ± SD of three independent experiments. * = $p < 0.05$ vs control cultures, Student's t test.

DOI: 10.1021/acsami.5b00481
ACS Appl. Mater. Interfaces 2015, 7, 7273–7281

stem cells. On the contrary, Lovmand et al.[45] demonstrated that osteogenic differentiation of MC3T3-E1 cells, a murine preosteoblastic cell line, was increased by smaller pillar and interpillar sizes. This discrepancy could be due to the differences in cell origin (mouse vs human), type (preosteoblastic cells vs MSCs), and size. We have not investigated at the molecular level how pillar features could affect cell behavior. However, as already demonstrated by several authors,[7,46] we can suppose that size, diameter, and spacing of microstructures can modify the tension and the arrangement of cytoskeletal fibers (actin and intermediate filaments) affecting signal transduction and, in turn, cell fate. Finally, our data indicate that the 4-10 surface seems to be the most effective microstructure for osteogenic differentiation. Starting from this evidence, we are planning to test other 4-10 surfaces with different peak heights.

■ ASSOCIATED CONTENT

Supporting Information

Spin-speed and FTIR graphs, SEM, optical images, and the photopolymerization scheme of the hybrid film. This material is available free of charge via the Internet at http://pubs.acs.org.

■ AUTHOR INFORMATION

Corresponding Author

*E-mail: giovanna.brusatin@unipd.it.

Author Contributions

The manuscript was written through contributions of all authors. All authors have given approval to the final version of the manuscript.

Notes

The authors declare no competing financial interest.

■ ACKNOWLEDGMENTS

The authors gratefully acknowledge CARIPLO for financial support through the projects "New materials for direct nanopatterning and nanofabrication by EUV and soft X-rays exposures". This work was supported by the Italian Ministry of Health (RF-2009-1528187).

■ REFERENCES

(1) Watt, F. M.; Huck, W. T. S. Role of the Extracellular Matrix in Regulating Stem Cell Fate. *Nat. Rev.* **2013**, *14*, 467.

(2) De Angelis, F.; Pujia, A.; Falcone, C.; Iaccino, E.; Palmieri, C.; Liberale, C.; Mecarini, F.; Candeloro, P.; Luberto, L.; De Laurentiis, A.; Das, G.; Scalac, G.; Di Fabrizio, E. Water Soluble Nanoporous Nanoparticle for in Vivo Targeted Drug Delivery and Controlled Release in B Cells Tumor Context. *Nanoscale* **2010**, *2*, 2230−2236.

(3) De Angelis, F.; Liberale, C.; Coluccio, M. L.; Cojoc, G.; Di Fabrizio, E. Emerging Fabrication Techniques for 3D Nano-Structuring in Plasmonics and Single Molecule Studies. *Nanoscale* **2011**, *3*, 2689−2696.

(4) Rehfeldt, F.; Engler, A. J.; Eckhardt, A.; Ahmed, F.; Discher, D. E. Cell Responses to the Mechanochemical Microenvironment—Implications for Regenerative Medicine and Drug Delivery. *Adv. Drug Delivery Rev.* **2007**, *59*, 1329−1339.

(5) Engler, A. J.; Sen, S.; Sweeney, H. L.; Discher, D. E. Matrix Elasticity Directs Stem Cell Lineage Specification. *Cell* **2006**, *126*, 677−689.

(6) Dalby, M. J.; Gadegaard, N.; Tare, R.; Andar, A.; Riehle, M. O.; Herzyk, P.; Wilkinson, C. D. W.; Oreffo, R. O. C. The Control of Human Mesenchymal Cell Differentiation using Nanoscale Symmetry and Disorder. *Nat. Mater.* **2007**, *6*, 997−1003.

(7) Yim, E. K.; Darling, E. M.; Kulangara, K.; Guilak, F.; Leong, K. W. Nanotopography-Induced Changes in Focal Adhesions, Cytoskeletal Organization, and Mechanical Properties of Human Mesenchymal Stem Cells. *Biomaterials* **2010**, *31*, 1299−1306.

(8) Benoit, D. S.; Schwartz, M. P.; Durney, A. R.; Anseth, K. S. Small Functional Groups for Controlled Differentiation of Hydrogel-Encapsulated Human Mesenchymal Stem Cells. *Nat. Mater.* **2008**, *7*, 816−823.

(9) Murphy, W. L.; McDevitt, T. C.; Engler, A. J. Materials as Stem Cell Regulators. *Nat. Mater.* **2014**, *13*, 547.

(10) Harrison, R. G. On the Stereotropism of Embryonic Cells. *Science* **1911**, *34*, 279−281.

(11) Flemming, R. G.; Murphy, C. J.; Abrams, G. A.; Goodman, S. L.; Nealey, P. F. Effects of Synthetic Micro- and Nano-Structured Surfaces on Cell Behavior. *Biomaterials* **1999**, *20*, 573−588.

(12) Pan, Z.; Yan, C.; Peng, R.; Zhao, Y.; He, Y.; Ding, J. Control of Cell Nucleus Shapes via Micropillar Patterns. *Biomaterials* **2012**, *33*, 1730−1735.

(13) Matsuzaka, K.; Walboomers, X. F.; Yoshinari, M.; Inoue, T.; Jansen, J. A. The Attachment and Growth Behavior of Osteoblast-Like Cells on Microtextured Surfaces. *Biomaterials* **2003**, *24*, 2711−2719.

(14) Recknor, J. B.; Recknor, J. C.; Sakaguchi, D. S.; Mallapragada, S. K. Oriented Astroglial Cell Growth on Micropatterned Polystyrene Substrates. *Biomaterials* **2004**, *25*, 2753−2767.

(15) Keselowsky, B. G.; Wang, L.; Schwartz, Z.; Garcia, A. J.; Boyan, B. D. Integrin Alpha(5) Controls Osteoblastic Proliferation and Differentiation Responses to Titanium Substrates Presenting Different Roughness Characteristics in a Roughness Independent Manner. *J. Biomed. Mater. Res., Part A* **2007**, *80A*, 700−710.

(16) Lucchetta, G.; Sorgato, M.; Zanchetta, E.; Brusatin, G.; Guidi, E.; Di Liddo, R.; Conconi, M. T. Effect of Injection Molded Micro-Structured Polystyrene Surfaces on Proliferation of MC3T3-E1 Cells. *eXPRESS Polym. Lett.* **2015**, *9*, 354−361.

(17) Chen, C. S.; Mrksich, M.; Huang, S.; Whitesides, G. M.; Ingber, D. E. Geometric Control of Cell Life and Death. *Science* **1997**, *276*, 1425−1428.

(18) Bruinink, A.; Wintermantel, E. Grooves Affect Primary Bone Marrow but Not Osteoblastic MC3T3-E1 Cell Cultures. *Biomaterials* **2001**, *22*, 2465−2473.

(19) Polini, A.; Pisignano, D.; Parodi, M.; Quarto, R.; Scaglione, S. Osteoinduction of Human Mesenchymal Stem Cells by Bioactive Composite Scaffolds without Supplemental Osteogenic Growth Factors. *PLoS One* **2011**, *6*, e26211.

(20) Dalby, M. J.; McCloy, D.; Robertson, M.; Agheli, H.; Sutherland, D.; Affrossman, S. Osteoprogenitor Response to Semi-Ordered and Random Nanotopographies. *Biomaterials* **2006**, *27*, 2980−2987.

(21) Martınez, E.; Engel, E.; Planell, J. A.; Samitier, J. Effects of Artificial Micro- and Nano-Structured Surfaces on Cell Behaviour. *Ann. Anat.* **2009**, *191*, 126−135.

(22) Kolind, K.; Dolatshahi-Pirouz, A.; Lovmand, J.; Pedersen, F. S.; Foss, M.; Besenbacher, F. A Combinatorial Screening of Human Fibroblast Responses on Micro-Structured Surfaces. *Biomaterials* **2010**, *31*, 9182−9191.

(23) Heckele, M.; Schomburg, W. K. Review on Micro Molding of Thermoplastic Polymers. *J. Micromech. Microeng.* **2004**, *14*, R1−R14.

(24) Zhang, N.; Chu, J. S.; Byrne, C. J.; Browne, D. J.; Gilchrist, M. D. Replication of Micro/Nano-Scale Features by Micro Injection Molding with a Bulk Metallic Glass Mold Insert. *J. Micromech. Microeng.* **2012**, *22*, 065019.

(25) Matschuk, M.; Bruus, H.; Larsen, N. B. Nanostructures for All-Polymer Microfluidic Systems. *Microelectron. Eng.* **2010**, *87*, 1379−1382.

(26) Midwoud, P. M.; Janse, A.; Merema, M. T.; Groothuis, G. M. M.; Verpoorte, E. Comparison of Biocompatibility and Adsorption Properties of Different Plastics for Advanced Microfluidic Cell and Tissue Culture Models. *Anal. Chem.* **2012**, *84*, 3938−3944.

(27) Johnson, A. S.; Anderson, K. B.; Halpin, S. T.; Kirkpatrick, D. C.; Spence, D. M.; Martin, R. S. Integration of Multiple Components

DOI: 10.1021/acsami.5b00481
ACS Appl. Mater. Interfaces 2015, 7, 7273−7281

in Polystyrene-Based Microfluidic Devices Part I: Fabrication and Characterization. *Analyst* **2013**, *138*, 129−136.
(28) Jaafar, I. H.,Ammar, M. M., Jedlicka, S. S., Coulter, J. P. Micro and Nanomolded Surface Structures for the Proactive Stimulation of Human Mesenchymal Stem Cell Differentiation, In *Polymer Process Engineering 09, Enhanced Polymer Processing* Coates, P., Ed.; University of Bradford: Yorkshire, United Kingdom, 2009; pp 294.
(29) Kjær, E. M.; Johansen, B. B.; Sørensen, H. H.; Rasmussen, H. K.; Arlø, U. R. Micro Injection Moulding. In *Proceedings of the 1st Euspen Topical Conference on Fabrication and Metrology in Nanotechnology*, De Chiffre, L., Carneiro, K., Eds.; IPL: Copenhagen, Denmark, 2000, Vol. *1*, pp 259−267.
(30) Alting, L.; Kimura, F.; Hansen, H.; Bissacco, G. Micro Engineering. *CIRP Annals−Manufacturing Technology* **2003**, *52*, 635−657.
(31) Sorgato, M.; Della Giustina, G.; Zanchetta, E.; Brusatin, G.; Lucchetta, G. Resins Materials as Alternative Insert for the Fabrication of Micro Structured Surfaces by Micro Injection Moulding. *Key Eng. Mater.* **2014**, *611−612*, 909−914.
(32) Brigo, L.; Zanchetta, E.; Della Giustina, G.; Brusatin, G. Hybrid Materials: A Bottom-Up Approach for Nanotechnology Applications. In *Nanophotonic Materials XI*, Cabrini, S.; Lérondel, G.; Schwartzberg, A. M.; Mokari, T., Eds.; Proc. SPIE—Int. Soc. Opt. Eng.: Bellingham, WA, 2014; Vol. *9161*, pp 91610B.
(33) Zanchetta, E.; Della Giustina, G.; Grenci, G.; Pozzato, A.; Tormen, M.; Brusatin, G. Novel Hybrid Organic−Inorganic Spin-on Resist for Electron- or Photon-Based Nanolithography with Outstanding Resistance to Dry Etching. *Adv. Mater.* **2013**, *25*, 6261−6265.
(34) Sha, B.; Dimov, S.; Griffiths, C.; Packianather, M. S. Micro-Injection Moulding: Factors Affecting the Achievable Aspect Ratios. *Int. J. Adv. Manuf. Technol.* **2007**, *33*, 147−156.
(35) Ricciardi, M.; Malpeli, G.; Bifari, F.; Bassi, G.; Pacelli, L.; Nwabo Kamdje, A. H.; Chilosi, M.; Krampera, M. Comparison of Epithelial Differentiation and Immune Regulatory Properties of Mesenchymal Stromal Cells Derived from Human Lung and Bone Marrow. *PLoS One* **2012**, *7*, e35639.
(36) Gregory, C. A.; Gunn, W. G.; Peister, A.; Prockop, D. J. An Alizarin Red-Based Assay of Mineralization by Adherent Cells in Culture: Comparison with Cetylpyridinium Chloride Extraction. *Anal. Biochem.* **2005**, *329*, 77−84.
(37) Decker, C. Photoinitiated Crosslinking Polymerisation. *Prog. Polym. Sci.* **1996**, *21*, 593−650.
(38) Tadanaga, K.; Ueyama, K.; Sueki, T.; Matsuda, A.; Minami, T. Micropatterning of Inorganic-Organic Hybrid Coating Films from Various Tri-Functional Silicon Alkoxides with a Double Bond in Their Organic Components. *J. Sol−Gel Sci. Techn.* **2003**, *26*, 431−434.
(39) Gardin, S.; Signorini, R.; Pistore, A.; Della Giustina, G.; Brusatin, G.; Guglielmi, M.; Bozio, R. Photocatalytic Performance of Hybrid SiO_2−TiO_2 Films. *J. Phys. Chem. C* **2010**, *114*, 7646−7652.
(40) Lucchetta, G.; Sorgato, M.; Carmignato, S.; Savio, E. Investigating the Technological Limits of Micro-Injection Molding in Replicating High Aspect Ratio Micro-Structured Surfaces. *CIRP Ann.−Manuf. Technol.* **2014**, *63*, 521−524.
(41) Dalby, M. J.; Gadegaard, N.; Oreffo, R. O. Harnessing Nanotopography and Integrin-Matrix Interactions to Influence Stem Cell Fate. *Nat. Mater.* **2014**, *13*, 558−69.
(42) Bacakova, L.; Filova, E.; Parizek, M.; Ruml, T.; Svorcik, V. Modulation of Cell Adhesion, Proliferation and Differentiation on Materials Designed for Body Implants. *Biotechnol. Adv.* **2011**, *29*, 739−67.
(43) Lavenus, S.; Ricquier, J. C.; Louarn, G.; Layrolle, P. Cell Interaction with Nanopatterned Surface of Implants. *Nanomedicine (London, U. K.)* **2010**, *5*, 937−47.
(44) Kolind, K.; Kraft, D.; Bøggild, T.; Duch, M.; Lovmand, J.; Pedersen, F. S.; Bindslev, D. A.; Bünger, C. E.; Foss, M.; Besenbacher, F. Control of Proliferation and Osteogenic Differentiation of Human Dental-Pulp-Derived Stem Cells by Distinct Surfacestructures. *Acta Biomater.* **2014**, *10*, 641−50.
(45) Lovmand, J.; Justesen, J.; Foss, M.; Lauridsen, R. H.; Lovmand, M.; Modin, C.; Besenbacher, F.; Pedersen, F. S.; Duch, M. The Use of Combinatorial Topographical Libraries for the Screening of Enhanced Osteogenic Expression and Mineralization. *Biomaterials* **2009**, *30*, 2015−22.
(46) Biggs, M. J.; Richards, R. G.; Gadegaard, N.; McMurray, R. J.; Affrossman, S.; Wilkinson, C. D.; Oreffo, R. O.; Dalby, M. J. Interactions with Nanoscale Topography: Adhesion Quantification and Signal Transduction in Cells of Osteogenicand Multipotent Lineage. *J. Biomed. Mater. Res., Part A* **2009**, *91*, 195−208.

DOI: 10.1021/acsami.5b00481
ACS Appl. Mater. Interfaces 2015, 7, 7273−7281